

# Evolution of Plastic Strain During a Flow Forming Process

M. J. Roy<sup>a,\*</sup> R. J. Klassen<sup>b</sup> J. T. Wood<sup>b</sup>

<sup>a</sup>*Dept. of Materials Engineering, The University of British Columbia, Vancouver, BC, Canada V6T 1Z4*

<sup>b</sup>*Dept. of Mechanical and Materials Engineering, The University of Western Ontario, London, ON, Canada N6A 5B9*

---

## Abstract

The distribution of equivalent plastic strain through the thickness of several AISI 1020 steel plates formed under different conditions over a smooth cylindrical mandrel using a single-roller forward flow forming operation was studied by measuring the local micro-indentation hardness of the deformed material. The equivalent plastic strain was higher at the inner and outer surfaces and lowest at the center of the workpiece. Empirical expressions are presented which describe the contribution of the roller and mandrel to the total local equivalent plastic strain within the flow formed part. The dependence of these expressions upon the thickness reduction during flow forming is discussed.

*Key words:* flow forming, shear forming, metal spinning, flow spinning, tube spinning, shear spinning, micro-indentation, micro-hardness, equivalent plastic strain, net shape manufacturing

---

## 1 Introduction

In a flow forming operation, a roller (or multiple rollers) are used to plastically deform the workpiece over the mandrel (Fig. 1). During this process, the material deforms both axially and circumferentially thereby simultaneously reducing the thickness and axially lengthening the work piece. The flow forming roller can have a unique profile and this geometry, combined with variable speeds and feeds, make a simultaneous multivariate analysis of the plastic strain induced in the workpiece very difficult. Gur and Tirosh (1982) stated that the flow forming process can be thought of as an operation involving the simultaneous extrusion (or drawing) and rolling of the workpiece. Characterization of both

---

\* Corresponding author.

*Email address:* majroy@interchange.ubc.ca (M. J. Roy).

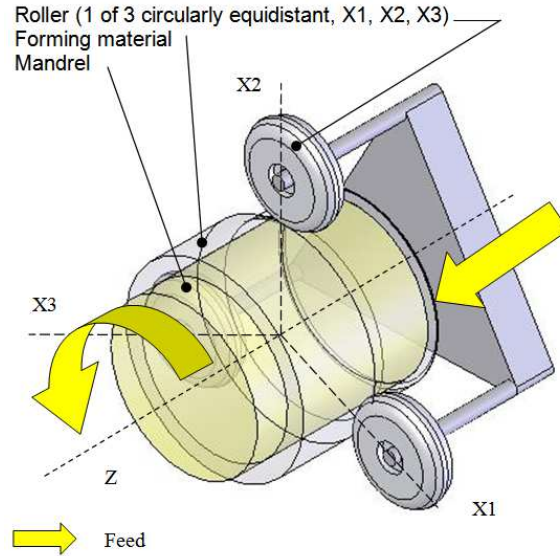


Fig. 1. Typical three-roller flow forming arrangement.

how, and the extent to which, the flow formed material deforms plastically during this process has not been extensively studied. While Kemin et al. (1997) and Xu et al. (2001) have adopted Finite Element Analysis (FEA) approaches to studying the deformation mechanisms prevalent during flow forming, there is little experimental work that has been conducted. As a result, there is a lack of understanding of both manufacturers and end-use designers of the mechanical properties of flow formed components, and sources of experimental data with which to validate FEA results.

The work presented in this paper is aimed at improving the understanding of the local plastic deformation induced in the workpiece during a single-roller flow forming process. While Brandon (1980) studied the strain distribution by inserting pins into a preform and observing how the pins displaced during forming, this work is aimed at measuring through-thickness equivalent strain directly. This is accomplished through experimentally mapping the local equivalent plastic strain through the thickness of a flow formed part using micro-indentation hardness measurements.

Micro-indentation techniques have been used by others to infer the local equivalent plastic strain of highly deformed materials. Chaudhri (1996, 2000) employed Vickers micro-indentation techniques to map the local equivalent plastic strain in the deformed region around a large spherical indentation made in copper while Tseng et al. (1998) also used a similar technique to map the equivalent plastic strain through the roll-bite region of cold rolled AISI 1018 steel. Two recent works detailing the macro-indentation hardness profiles through the thickness of flow formed ferritic steel workpiece alloys were published by Chen and Jones (2002) and Gur and Arda (2003), however neither of these investigations correlated the measured hardness to the equivalent plastic strain.

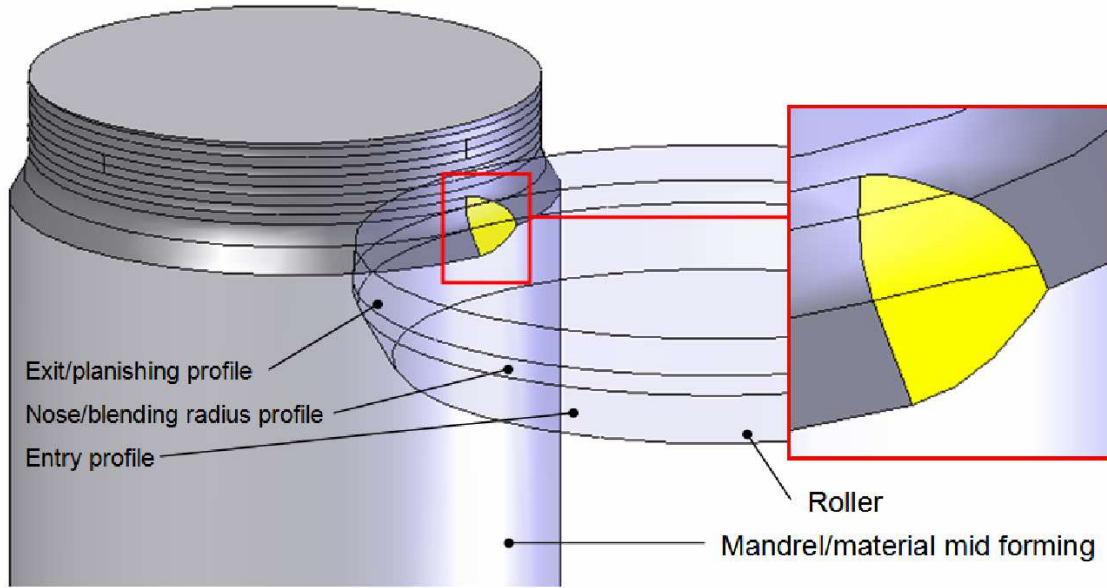


Fig. 2. Single roller contact in flow forming showing the mandrel/workpiece and key roller profiles.

## 2 Experiment Details

Single-roller flow forming operations were performed over a smooth cylindrical mandrel using a roller with an outer surface profile consisting of two flat regions and a blending radius between them (Fig. 2). Three passes (Fig. 3, 4) of the roller were used to form flat circular blanks of AISI 1020 steel plate, of 8.5 mm initial thickness, over the mandrel. During the first pass, the part did not contact the mandrel; this is essentially a classical metal spinning operation. The second pass involved minimal contact of the workpiece with the mandrel. The work piece was in full contact with the mandrel throughout the third pass. The forming process was stopped in the middle of the third pass by quickly retracting the roller away from the work piece. This was done to investigate the local deformation of the steel in the region ahead of the roller. In total, six tests were performed. The first two forming passes of each test were performed under the same conditions. The thickness reduction for the first pass was 6% and the second pass was 29%, while the third pass was performed at six different thickness reduction levels, resulting in a total thickness reduction ranging from 48.2 to 55.3%.

Each flow formed part was inspected to find the final roller position on the part. The part was then sectioned at this point and mechanically polished to  $< 1\mu\text{m}$  surface roughness in preparation for micro-indentation hardness testing. Depth controlled micro-indentation hardness data were collected from the polished as-received 1020 steel and from the flow formed parts using a Berkovich microindentation hardness tester manufactured by Micro Materials Ltd. (Wrexham, UK). It was found that the optimal indentation spacing was  $100\mu\text{m}$ , and the optimal indentation depth was  $\sim 7\mu\text{m}$ .

Three rows of indentations were made on each of the six samples. Since the objective of

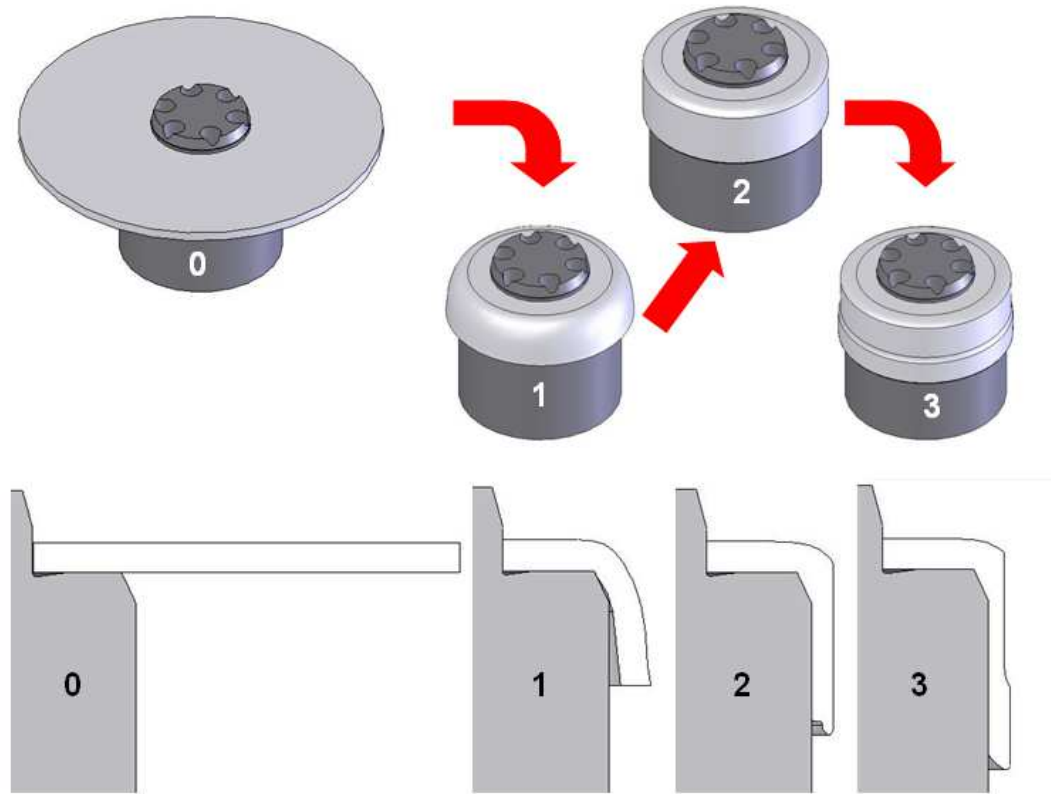


Fig. 3. Flow forming sequence showing (0) starting material, (1) ‘cupped’ material, (2) first forming pass and (3) later pass frozen mid-forming.

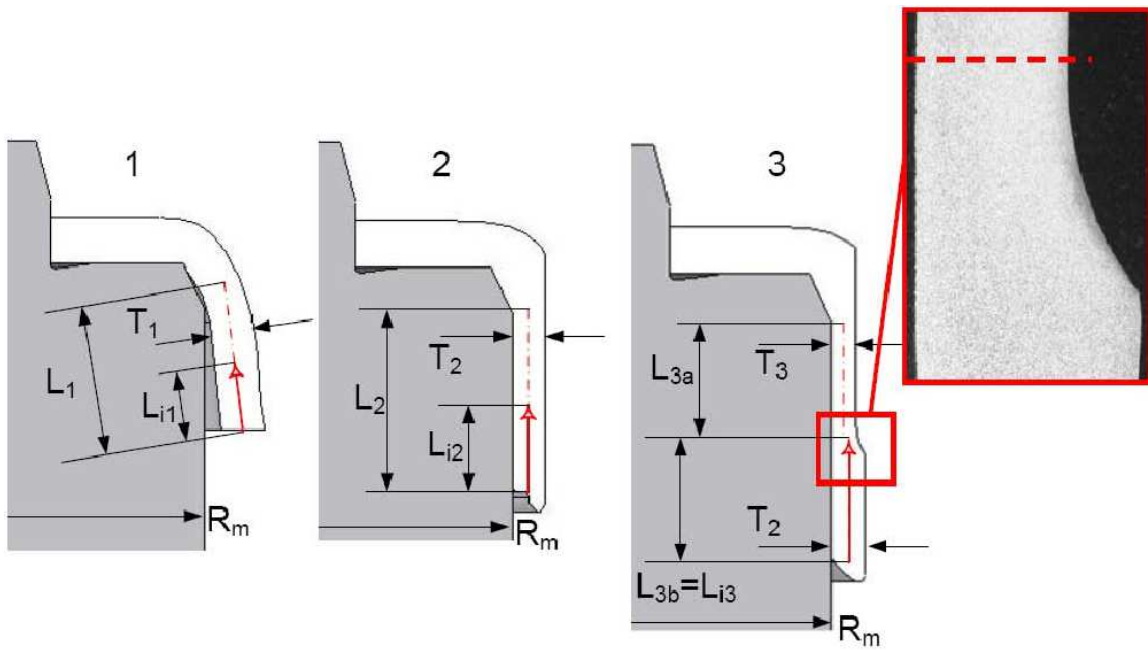


Fig. 4. Indentation location at distance  $L_i$  from the base of each of the three successive parts shown in Fig. 3.

the indentation testing was to characterize the evolution of the local plastic strain at a specific location within the workpiece and since the workpiece was incrementally deformed through multiple flow forming passes, the specific location,  $L_i$  of the indentations (Fig. 4), must be different for each successive forming pass. This was done to guarantee that the indentations are made in the same location within the workpiece. Assuming that work piece volume is conserved during the deformation, and using the known dimensions  $T_1$ ,  $T_2$ ,  $T_3$ ,  $L_{3a}$  and the mandrel radius,  $R_m$ , the location of the central rows of indents  $L_{i1}$  and  $L_{i2}$  were calculated (Fig. 4). This assumes that the work piece geometry evolves through each of the forming passes as a hollow cylinder becoming both thinner and longer.

### 3 Correlating Micro-Indentation Hardness to Equivalent Plastic Strain

The correlation of the Berkovich hardness values to equivalent plastic strain was accomplished by deforming as-received AISI 1020 steel plate to different levels of plastic strain through cold-rolling and uniaxial tensile deformation. Seven specimens were treated in this manner with true plastic strain from rolling ranging from 0.25 to 0.40. For small strain levels, five tensile specimens were cut directly from as received material. The tensile tests were conducted on a Instron 8804 servo-hydraulic test platform according to standard procedures (ASTM 370), with specimens having a gauge length of 50.8 mm. For all tensile tests, the extension rate was set at 2 mm per minute, and the specimen extension was continually monitored with a clip-on type extensometer.

The tensile specimens were then sectioned and polished. The same micro-indentation procedure was then performed on these samples as was performed on the flow formed samples. Rows of indentations were made in locations through the thickness, outside of the necked regions of the sectioned tensile samples, on surfaces whose normal was perpendicular to the rolling direction. A minimum of 38 indents up to a maximum of 50 indents per sample were made to render statistically significant results in locations that such that all indents were made far enough away from the edges of the tensile specimen that they were not affected by surface/corner inhomogeneity of the plastic strain. Fig. 5(a) shows the measured Berkovich hardness plotted against the equivalent plastic strain for both the cold-rolled specimens and the uniaxially deformed tensile specimens. As the micro-indentation scheme selected was one which minimized indentation depth to minimize the spacing between the indentations, the effect of local mechanical anisotropy of the steel appears in the form of scatter in the measured hardness. The error bars on the average hardness data in Fig. 5 indicate one standard deviation of variance in the measured hardness about the calculated mean hardness value. While the average percentage variation in the hardness is about 8% at any given value of equivalent plastic strain, this percentage rises to 16% when the plastic strain is low. For the highly deformed rolled specimens, the scatter is diminished and about 4%. This scatter is inherent for this type of measurement, as the measured indentation hardness is an average of the yield properties of all the grains that are deformed in the immediate region around the indentation. Since the rolling process compresses the grain size through the thickness

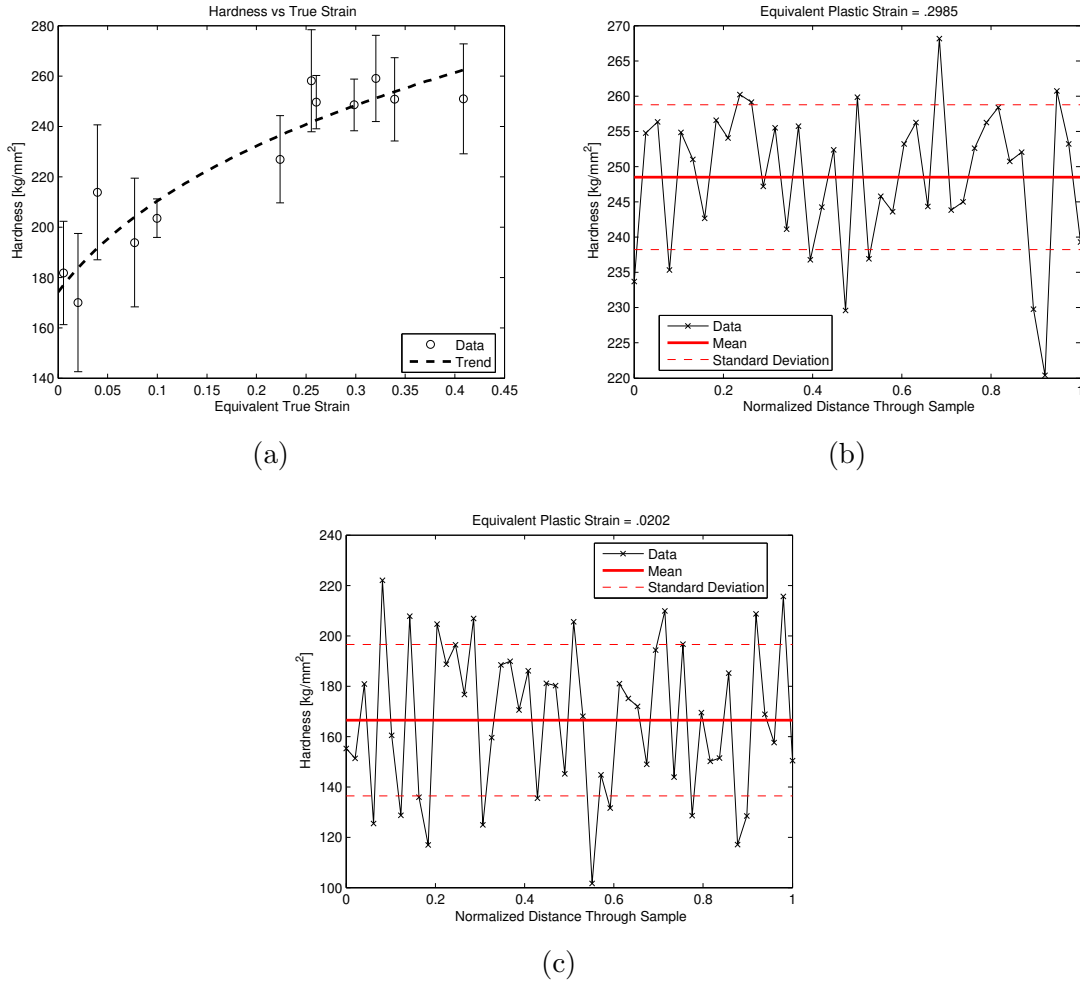


Fig. 5. (a) Indentation hardness versus true equivalent plastic strain of AISI 1020 steel tensile samples cold rolled to various levels of equivalent plastic strain prior to tensile testing. Error bars are  $\pm 1$  standard deviation from mean hardness values, and show inherent scatter from  $\pm 4\%$  at high strains to  $\pm 16\%$  at low strains. The sample with both the highest scatter at a strain of 0.0202 (b) and the lowest scatter at a strain of 0.2985 (c) are shown with hardness values plotted versus normalized distance through the thickness of the sample.

of the sample normal to the rolling direction, indentations made in the rolled material interact with more grains resulting in a measured hardness that displays less scatter from indentation-to-indentation. Figures 5(b) and (c) show the hardness plotted across the normalized sample thickness for both high and low strain samples.

Following the work of Tabor (1951), it was found that the correlation of the Berkovich microhardness with the equivalent plastic strain,  $\varepsilon$ , can be fitted with the following expression.

$$H(\varepsilon) = A(\varepsilon + \varepsilon_{ind})^n \quad (1)$$

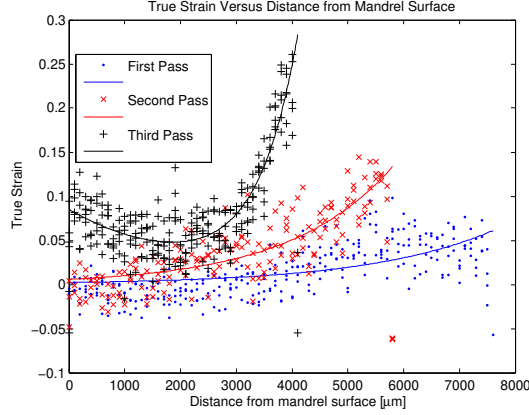


Fig. 6. True equivalent plastic strain found from Berkovich micro-hardness testing versus distance from mandrel surface for three forming passes resulting in a 50.5% total reduction.

In this equation,  $H$  is the Berkovich hardness in  $\text{kg}_f/\text{mm}^2$  at depth of  $\sim 7 \mu\text{m}$ ,  $A$  and  $n$  are material constants and  $\varepsilon_{ind}$  is the additional average equivalent plastic strain associated with the indentation process. These parameters were all derived from curve-fitting to the data in Fig. 5. The trend acquired in this manner described the experimental results within  $\pm 1$  standard deviation with an  $R^2$  value of 0.85 ( $R^2$  value of 1 being a perfect fit) and a Standard Square Error of 1.74E03. Rearranging Eq. 1 and substituting the fitted terms  $A$ ,  $n$  and  $\varepsilon_{ind}$  gives the following expression for the average equivalent plastic strain as a function of hardness.

$$\varepsilon(H) = \left( \frac{H}{307.1} \right)^{4.673} - 0.0707 \quad (2)$$

The fitted term  $\varepsilon_{ind} = 0.0707$  is close to  $\varepsilon_{ind} = 0.08\%$  reported by Tabor (1951) for pyramidal indentations made in low carbon steel.

## 4 Results

The hardness profiles from the flow formed samples were translated to equivalent true plastic strain using Eq. 2. Fig. 6 shows the results of this translation for samples deformed with one to three flow forming passes.

For the first pass, the work piece is only acted on by the roller; the mandrel does not contact the workpiece. The equivalent plastic strain at the mandrel surface is therefore approximately zero (Fig. 6). During the second pass there is minimal contact between the workpiece and the mandrel, the equivalent plastic strain is close to zero at the mandrel surface and increases up to about 15% toward the roller side of the work piece. During the third pass, the work piece is in full contact with the mandrel and there is a marked increase, up to about 10 %, in equivalent plastic strain at the mandrel surface. The plastic

strain at the roller side of the work piece is much greater than the previous pass due the large additional plastic strain imparted in the third pass.

While micro-indentation is a robust way of measuring local equivalent plastic strain, and has been used for this purpose by other researchers, the magnitude of the local plastic strain is also reflected in local changes in grain size and shape in the deformed part. Scanning electron microscopy (SEM) was therefore used to record the local grain shape around indentations in order to confirm that the variation in local equivalent plastic strain, measured by the micro-hardness technique, coincided with the observed change in local grain size and shape. The SEM analyses were performed on indented, third pass flow formed samples that were etched in a 10% nital solution for 5 seconds after the indentations were made (Fig. 7).

At the roller surface, the grains are much more refined in the thickness direction and elongated in the axial direction than at the minimum strain location in the center of the material. The grains at the mandrel surface are more refined than at the minimum strain location, but less than at the roller surface. This change in grain morphology agrees with the known nature of flow forming deformation as published by Chen and Jones (2002) and Gur and Arda (2003); namely the rollers compress the material in the thickness direction while elongating it in the axial direction. Also apparent in Fig. 7 is the relative size of the indentations; smaller indentations correlate to higher degrees of grain refinement and elongation. The microstructure observations therefore corresponds to the trends shown in Fig. 6.

## 5 The Effect of the Roller and Mandrel on the Local Equivalent Plastic Strain

The data in Fig. 6 can be used to derive expressions relating the evolution of the equivalent true strain across the thickness of a flow formed AISI 1020 steel work piece. This is accomplished by plotting the equivalent plastic strain versus normalized thickness across the work piece and expressing the profiles in the form of exponential relationships (Eq. 3-6). This allows for the best possible expression while minimizing the number of empirical terms to describe the effects of both the roller and mandrel's influence on the material.

For the first pass, plastic strain due to the influence of the roller,  $\varepsilon_{1r}(x)$  is imparted to the material, as shown in Eq. 6, where  $x$  is the normalized distance from the mandrel. For the second pass, the strain developed in the first pass is added to by the second pass of the roller,  $\varepsilon_{2r}(x)$ . It should be noted that it is assumed that there is minimal contact of the workpiece with the mandrel during the first and second roller passes, and as such  $\varepsilon_{1m}(x) = 0$  and  $\varepsilon_{2m}(x) = 0$ . This assumption is validated by the experimental data in Fig. 6 that show essentially no equivalent plastic strain at the mandrel surface for these passes. For the third pass, the workpiece is in complete contact with both the roller and the mandrel. Therefore, the equivalent plastic strain is added to by contributions from both the roller and the mandrel,  $\varepsilon_{3r}(x)$  and  $\varepsilon_{3m}(x)$ .



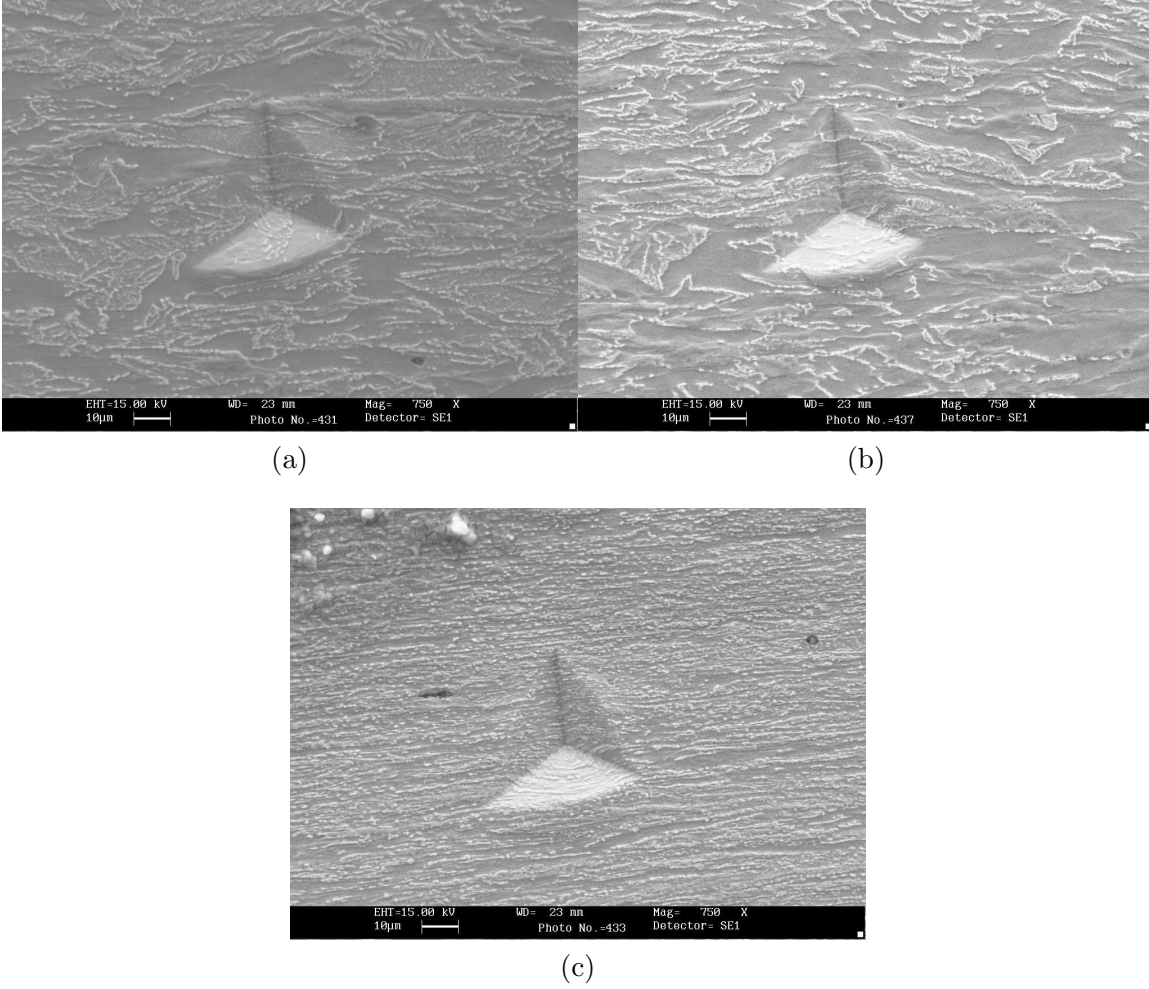


Fig. 7. SEM images of Berkovich indentations through at (a) close to the mandrel interface, (b) minimum hardness and (c) close to the roller interface of a flow formed work piece. Local grain elongation is apparent, as is small decrease in the relative size of the indentations in areas where the grain elongation is largest.

$$\varepsilon(x) = \sum_{i=0}^n \varepsilon_i(x) \quad (3)$$

$$\varepsilon_i(x) = \varepsilon_{im}(x) + \varepsilon_{ir}(x) \quad (4)$$

$$\varepsilon_{im}(x) = \frac{A_{im}\Delta t}{t_o} \exp\left(\frac{B_{im}x}{t_o - \Delta t}\right) \quad (5)$$

$$\varepsilon_{ir}(x) = \frac{A_{ir}\Delta t}{t_o} \exp\left(\frac{B_{ir}x}{t_o - \Delta t}\right) \quad (6)$$

Where  $x$  is the normalized thickness,  $\varepsilon(x)$  is the equivalent plastic strain as a function of the normalized thickness,  $n$  is the total number of forming passes,  $i$  is each forming step.  $\varepsilon_{2i}(x)$  is the equivalent plastic strain occurring at each forming step and can be further-

more expressed as the sum of  $\varepsilon_{im}(x)$ , the equivalent plastic strain due to the mandrel, and  $\varepsilon_{ir}(x)$ , the equivalent plastic strain due to the roller at each forming step. For the formulations of  $\varepsilon_{im}(x)$  and  $\varepsilon_{ir}(x)$  (Eqns. 5 and 6),  $A_{im,ir}$  and  $B_{im,ir}$  are fitted empirical coefficients, while  $\Delta t$  and  $t_o$  are the change in thickness and the starting thickness, respectively.

Through normalization, the coefficients achieved through fitting,  $A_{im,ir}$  and  $B_{im,ir}$  (Table 1) are dependent on process conditions and the length along the part,  $L_i$ , and not strain. Note that the coefficients used for the first and second forming pass were derived from the first and second pass data from the sample with 55.3% reduction.

Table 1

Fitted coefficients to Eq. 3 at various reduction levels with confidence boundaries and Sum of Squared Error (SSE). Third pass results are averaged over all six samples.

Sample	Coefficient	Value	
		(95% confidence bounds)	SSE
First pass	$A_{1r}$	4.10E-01 ( $\pm 1.27E-03$ )	0.1634
	$B_{1r}$	4.20 ( $\pm 1.11E-01$ )	
Second pass	$A_{2r}$	4.20E-03 ( $\pm 1.96E-03$ )	0.1148
	$B_{2r}$	1.60 ( $\pm 3.05E-01$ )	
Third pass	$A_{3m}$	1.90E-01 ( $\pm 2.75E-02$ )	0.3711
	$B_{3m}$	-1.31 ( $\pm 6.52E-01$ )	
	$A_{3r}$	5.54E-04 ( $\pm 6.23E-04$ )	
	$B_{3r}$	8.06 ( $\pm 1.84$ )	

Each of the terms in Eq. 3 are a function of process parameters such as roller geometry, mandrel geometry, the rate of axial roller movement, the mandrel rotational velocity and the degree of thickness reduction per pass. In this investigation, only the effect of thickness reduction ratio during the third and final pass is assessed while all other variables are held constant. Fig. 8 shows  $\varepsilon_{3r}(x)$  and  $\varepsilon_{3m}(x)$  versus through-thickness distance,  $x$ , from the mandrel surface for the thickness reductions ranging from 48.2% to 55.2%. Note that the relationships derived here are based upon data obtained by using Eqn. 2, and therefore are subject to an additional average scatter of about  $\pm 8\%$  resulting in the measured indentation hardness for samples containing a fixed value of average equivalent plastic strain (Section 3).

For the thickness reduction levels investigated, the shape of the trend  $\varepsilon_{3m}(x)$  essentially stays constant. For the roller side, the change in the equivalent plastic strain versus position profile is more dramatic with the gradient increasing as the thickness reduction is

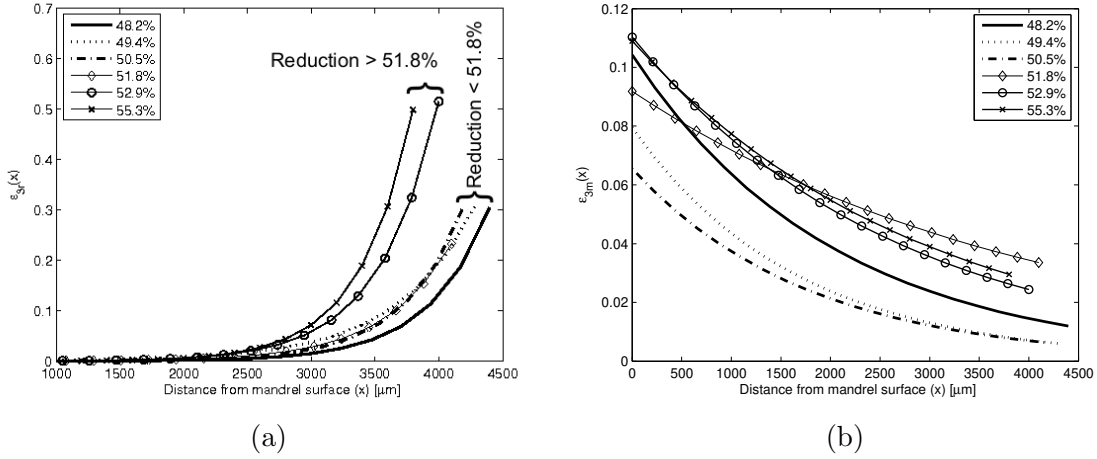


Fig. 8. Equivalent plastic strain trends through the thickness of a flow formed workpiece at three different reduction levels.  $\varepsilon_{3r}(x)$ , shown in (a) is a function due to the roller, and  $\varepsilon_{3m}(x)$ , shown in (b), is a function due to the mandrel. A critical reduction level past 51.8% results in a large increase in  $\varepsilon_{3r}(x)$ .

increased. The presence of extreme strain gradients in forming operations often leads to defects in the final product. The presence of large strain gradients after a critical reduction level suggests that there is a maximum thickness reduction level at which the material can be flow formed and still remain defect free. This was found to occur at a reduction level between 51.8% and 52.9%. The overall distribution of strain changes abruptly, as shown in Fig. 8(b), leading to an increase in maximum strain of 0.2 at the roller interface. This is shown in Fig. 9, where the maximum strain at the roller interface versus reduction level shows an abrupt shift as the thickness reduction level passed between these two values. At reduction values beyond 51.8%, defects, in the form of localized cracking on the roller-side surface of the formed part were observed. As indentation testing was conducted away from these defects, the presence of these defects do not affect the findings of this paper. The size, scale and evolution of these defects remain the subject of on-going research.

## 6 Conclusions

Micro-indentation hardness testing was successfully employed to map the true equivalent plastic strain through the thickness of a flow formed AISI 1020 steel work piece that was deformed by a three-stage single roller, forward flow forming process. The work piece experienced increased plastic strain in subsequent forming passes with material near the mandrel and the roller displaying elevated equivalent plastic strain, which was dependent upon thickness reduction, during the final forming stage. This coincided with the onset of complete contact between the work piece and the mandrel. It was also observed that as reduction increased, the local plastic strain increased more rapidly at the roller interface than at the mandrel interface. This trend increased very rapidly past a critical reduction level found to be between 51.8 and 52.9%. Therefore, it is suggest that since there is a

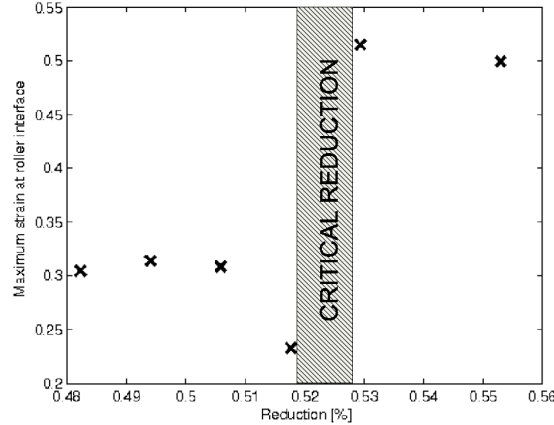


Fig. 9. Maximum equivalent plastic strain incurred at the roller interface found from fitted relationships versus thickness reduction level. The strain increases substantially at a critical reduction level between 51.8% and 52.9% indicated by the vertical bar.

substantial increase in plastic strain at the roller interface when the thickness reduction is about 52%, this represents the maximum equivalent plastic strain that can be imparted to the 1020 steel by flow forming prior to the onset of roller-induced defects on the surface of the workpiece. This characterization of roller-induced defects created during high-strain flow forming is the subject of further investigation.

In summary, this investigation has presented a characterization of the effect of the roller, the mandrel and thickness reduction process parameter on the evolution of the local equivalent plastic strain in a work piece during flow forming. The approach and results of this investigation allows to validate further FEA modeling approaches as well as for end users of flow formed components to understand and quantify the mechanical properties of flow formed parts.

## References

- Chaudhri, M. M., 1996. Subsurface plastic strain distribution around spherical indentations in metals. *Physica Status Solidi (a)* 74, 1213–1224.
- Chaudhri, M. M., 2000. Strain hardening around spherical indentations. *Physica Status Solidi (a)* 182, 641–652.
- Chen, Y., Jones, A., 2002. The microstructure and recrystallization of flow-formed oxide-dispersion-strengthened ferritic alloy: Part i. deformation structure. *Metallurgical and Materials Transactions A* 33A, 3777–3785.
- Gur, C. H., Arda, E. B., 2003. Effect of tube spinning and subsequent heat treatments on strength, microstructure and residual stress state of aisi/sae type 4140 steel. *Materials Science and Technology* 19, 1590–1594.
- Brandon, D. G., Ari-Gur, P., Bratt, Z., Gur, M., 1980. Texture inhomogeneity and the strain distribution in shear-spun steel tubes. *Materials Science and Engineering* 44, 185–194.

- Gur, M., Tirosh, J., 1982. Plastic flow instability under compressive loading during shear spinning process. *Journal of Engineering for Industry* 104, 17–22.
- Kemin, X., Zhen, W., Yan, L., Xianming, Z., 1997. The disposal of key problems in the fem analysis of tube stagger spinning. *Journal of Materials Processing Technology* 69, 176–179.
- Tabor, D., 1951. *The Hardness of Metals*. Clarendon Press, Oxford.
- Tseng, A. A., Wang, S. R., Lau, A. C. W., 1998. Local variations of strain and strain rate in roll bite region during rolling of steels. *Transactions of the ASME* 120, 86–96.
- Xu, Y., Zhang, S. H., Li, P., Yang, K., Shan, D. B., Lu, Y., 2001. 3D rigid-plastic FEM numerical simulation on tube spinning. *Journal of Materials Processing Technology* 113, 710–713.